Advances in Complex Systems, Vol. 9, No. 4 (2006) 353–367

World Scientific
www.worldscientific.com

ON MODELING COMPLEX COLLECTIVE BEHAVIOR IN MYXOBACTERIA

YI JIANG

Theoretical Division, Los Alamos National Laboratory,
Los Alamos, NM 87545, USA
jiang@lanl.gov

OLGA SOZINOVA* and MARK ALBER†

Department of Mathematics and Center for the Study of Biocomplexity,
University of Notre Dame, Notre Dame, IN 46556, USA
**osozinov@nd.edu*
†*malber@nd.edu*

Received 13 September 2005
Revised 16 February 2006

This paper reviews recent progress in modeling collective behaviors in myxobacteria using lattice gas cellular automata approach (LGCA). Myxobacteria are social bacteria that swarm, glide on surfaces and feed cooperatively. When starved, tens of thousands of cells change their movement pattern from outward spreading to inward concentration; they form aggregates that become fruiting bodies. Cells inside fruiting bodies differentiate into round, nonmotile, environmentally resistant spores. Traditionally, cell aggregation has been considered to imply chemotaxis, a long-range cell interaction. However, myxobacteria aggregation is the consequence of direct cell-contact interactions, not chemotaxis. In this paper, we review biological LGCA models based on local cell–cell contact signaling that have reproduced the rippling, streaming, aggregating and sporulation stages of the fruiting body formation in myxobacteria.

Keywords: Myxobacteria; collaborative behavior; cellular automata; pattern formation; complex systems; stochastic modeling.

1. Introduction

Myxobacteria are found in cultivated soils all over the earth. Their biological success is due to social behavior that resembles the cellular slime molds (*Dictyostelium discoidium* in particular) and, to some extent, development in animals and plants [12]. Myxobacteria move by gliding across the surface of soil particles, or of agar in the laboratory. They feed on colonies of other bacteria like packs of microbial wolves; each myxobacterial cell, after surrounding a colony and secreting hydrolytic enzymes that digest the prey, shares the products of hydrolysis with its mates. Since they compete with many other micro-predators in soil, their food supply is often

depleted. As they approach nutrient depletion, myxobacterial cells stop growing and use a quorum sensor to communicate with each other. If a quorum is present, the cells undergo a multi-stage morphological process which requires an organized, collective effort of tens of thousands of cells, culminating in formation of a multicellular fruiting body.

The modes of cell–cell communication that lead to myxobacterial fruiting bodies are quite unique. Myxobacteria use two cell–cell signals. First, they employ the diffusible, quorum-sensing A-signal to certify the presence of enough cells to build a fruiting body. Then the C-signal, the cell-surface-bound signaling protein, is exchanged during cell–cell contacts. Depending on the level of C-signal, a cell switches its behavior from frequently reversing its traveling direction to consistently following other cells [31]. Cell response to different levels of the C-signal is also responsible for sporulation.

The rather sophisticated social life of myxobacteria facilitates more efficient digestion of food, ensures their long-term survival by differentiating into spores and helps spore dispersion [16]. Cooperation through cell–cell signaling is the key to maintaining their social stability. Indeed, when cheater mutants that fail to produce the C-signal are mixed with the wild-type strains, the social exploitation can destabilize the cooperative system and increase the risk of extinction [8].

This review emphasizes a cell based approach to stochastic lattice gas cellular automaton (LGCA) modeling of different types of collective behavior in myxobacteria. Unlike the slime mold *Dictyostelium*, whose developmental patterns have been modeled as an excitable media due to signal diffusion, relay, and cell chemotaxis [9], the development of myxobacteria is governed by direct cell–cell interactions rather than chemotaxis. Studying myxobacteria fruiting body formation provides one with new insight into the collective microbial behaviors.

2. Myxobacteria Morphogenesis

Myxobacteria are elongated, rod-shaped cells with a 7:1 length to width ratio (typically 2 to 12 by 0.7 to 1.2 μm [26]), as illustrated in the left panel of Fig. 1. They move on surfaces by gliding along their long axis [7]. They move in one direction for awhile and then reverse the direction of their movement. Two molecular motors, retractile grappling hooks at their leading end (S-motility) [25] and jets for secreting a polysaccharide gel at the trailing end (A-motility) [35], provide them with thrust.

The C-signal, a 17-kDa cell-surface-associated protein [23], coordinates cell movement during fruiting-body development. C-signal is exchanged when a pair of cells makes end-to-end contact with each other [18]; side-by-side or end-by-side contacts do not exchange signal. When development starts, there are few C-signal molecules per cell, and cells making end-to-end contact respond to signal exchange by reversing their direction of gliding [34]. Regular reversals generate the *ripple pattern*.

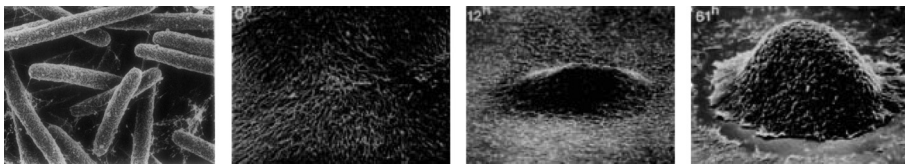

Fig. 1. Left: Scanning electron microscope image of *M. xanthus* (from Ref. 5 with permission); 2nd to 4th, Snapshots during the fruiting body formation of *M. xanthus* at 0 h, 12 h, and 61 h (from Ref. 21 with permission).

However, each time C-signal is exchanged, a positive feedback loop elevates the number of signal molecules on signaling cells. Different levels of C-signal, encoded by the csgA gene, induce the different stages of fruiting body formation [19, 20, 22]. The expression of csgA is controlled by two feedback loops in the signal transduction pathway, one of which is caused by the increased density and alignment in response to C-signal [14, 19, 22]. The second is an intracellular loop via the act operon [10]. Each time a cell receives the C-signal it increases expression of csgA.

After cells have accumulated 25–50 C-signal molecules, instead of reversing in response to C-signal exchange, they respond by suppressing reversal and continuing to move in the same direction. When the end of a cell nudges the cell ahead of it, this response causes the cells to move as a chain [13]. A chain of many cells moving in the same direction is a *stream*.

Myxobacterial aggregation begins with the formation of stationary traffic jams involving hundreds of cells (Figs. 1(b) and (c)). When cells moving in opposite directions happen to meet in a small area, they stall at the points of collision if they are prevented from turning by other cells at their side or behind them. In the experiment with cells submerged in culture [21], cells first settle on the bottom of the culture and immediately form domains of cells (facet patterns) [21], where cells align roughly parallel to each other within each domain while different domains have different orientations. Traffic jams form at intersections of two domains [17]. Such jammed cells remain stationary for several hours. The system then enters a second stage of aggregation, after cells have elevated their C-signal levels and have begun to stream. As a stream of cells approaches a traffic jam, it glides over or around the jam, treating the jam as if it were an inanimate lump. The stream of cells must bend as it passes over or around the jam and thus initiates a roughly circular orbit. Within a stable aggregate, a sub-population of cells differentiate into round spores.

3. Biological LGCA Models

LGCA models employ a regular, finite lattice and include a finite set of particle states, an interaction neighborhood and local rules that determine the particles' movements and transitions between states. In classical LGCA, particles (biological cells) are dimensionless and represented as a single occupied node on a lattice

(e.g. see Refs. 6 and 24). The connectivity of the lattice fixes the number of allowed non-zero velocities or channels for each particle. For example, a nearest-neighbor square lattice has four non-zero allowed channels. The channel specifies the direction and magnitude of movement, which may include zero velocity (resting). In a simple exclusion rule, only one particle may have each allowed non-zero velocity at each lattice site. Thus, a set of Boolean variables describes the occupation of each allowed particle state: occupied (1) or empty (0).

Simplified cell representation in the form of one particle is not enough for a sophisticated model of myxobacteria fruiting body formation. Also, a realistic model of cell overlap and cell stacking is needed since interaction occurs only at specific regions of highly elongated cells and cell density is a critical parameter throughout the morphogenesis.

In Secs. 3.1–3.3, we use 2-D and 3-D LGCA models based on an extended cell representation [1–4, 32]. Namely, each cell is represented as (i) a single node which corresponds to the position of the cell's center (or "center of mass"), (ii) the choice of occupied channel at the cell's position designating the cell's orientation and (iii) a local neighborhood defining the physical size and shape of the cell with associated interaction neighborhoods (see Fig. 2). Cells can bend by small angles. The interaction neighborhoods depend on the dynamics of the model and need not to exactly overlap with the cell shape. Representing a cell as an oriented point with an associated cell shape is computationally efficient, yet approximates cell dynamics more closely than assuming point-like cells, since elongated cells may overlap in many ways. We have also solved the cell stacking problem, since overlapping cell shapes correspond to cells stacked on top of each other. This cell representation conveniently extends to changing cell dimensions and the more complex interactions during fruiting body formation.

3.1. *Rippling*

Rippling is one of the most interesting patterns that develops during myxobacteria morphogenesis. Rippling often, but not necessarily, occurs spontaneously and transiently during aggregation [30, 34]. Rippling myxobacteria form equidistant ridges of high cell density which appear to advance through the population as rhythmically traveling waves [30] (Fig. 3). Cell movement in a ripple is approximately one-dimensional since the majority of cells are aligned and move in parallel lines with or against the direction of wave propagation [29]. Tracking individual bacteria within a ripple has shown that cells reverse their traveling directions back and forth and that each travels on the order of one wavelength between reversals [29]. The ripple waves propagate with no net transport of cells [29] and wave overlap causes neither constructive nor destructive interference [29].

Sager and Kaiser [29] have proposed that precise reflection explains the lack of interference between wave-fronts in myxobacteria rippling. Oriented collisions between cells initiate C-signaling that causes cell reversals. According to this

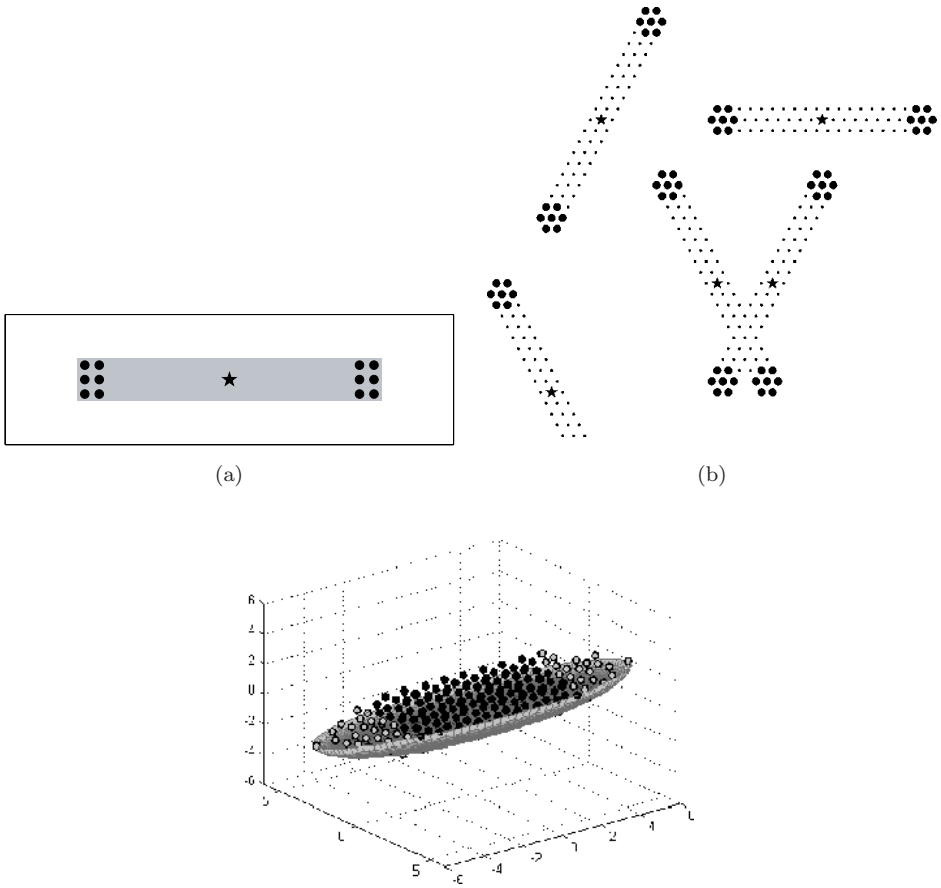

Fig. 2. Cell representations for (a) 2D square lattice model for rippling, and (b) 2D triangular lattice model for aggregation. Stars indicate cell center and pixels of darker shades of gray indicate the C-signaling neighborhoods at cell poles. (c) A 3D representation in the form of an ellipsoid on a triangular lattice used for modeling aggregation and sporulation. Pixels of lighter gray indicate cell poles.

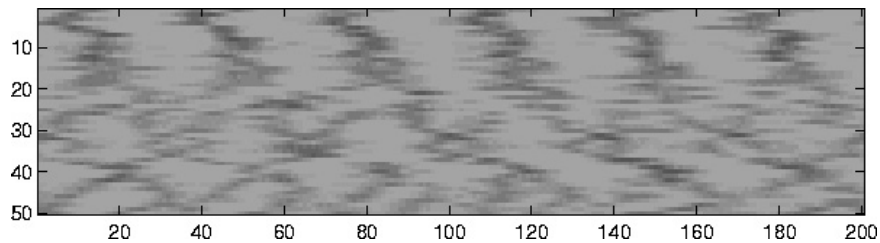

Fig. 3. Typical ripple pattern including both a cell clock and refractory period in the model. (Cell length $= 5$, $\delta = 2$, $R = 10$, $t = 15$, $\tau = 25$.) Figure shows the density of cells (darker gray indicates higher density) on a 50×200 lattice after 1,000 time steps, corresponding to approximately 200 minutes in real time. (From Ref. 1 with permission.)

hypothesis of precise reflection, when two wave-fronts collide, the cells reflect one another, pair by pair, in a precise way that preserves the wave structure in mirror image.

Models for rippling described in Refs. 6, 11 and 24 assume precise reflection. Key differences among these models include their biological assumptions regarding the existence of internal biochemical cell cycles. With completely different assumptions, these models all qualitatively produce ripple patterns resembling experiment.

To resolve the conflicts of these models for rippling our LGCA model was designed to test different assumptions [1]. In our models for rippling and aggregation, we define the size and shape of the cell as a $3 \times \ell$ rectangle, where ℓ is cell length. As ℓ increases, the cell shape becomes more elongated. A cell length of $\ell = 30$ corresponds to the 1×10 proportions of rippling *Myxococcus xanthus* cells [18]. An *internal timer* is a hypothetical molecular cell clock which regulates the interval between reversals. The *refractory period* is a period of time immediately following a cell reversal, during which the cell is insensitive to C-factor. Although there is no evidence of a refractory period in the C-signaling system, the refractory period is a general feature of bacterial signaling systems [11].

In the model described in Ref. 1, cells are initially randomly distributed on a square lattice with periodic boundary conditions with density δ, where δ is the total cell area divided by total lattice area. Every cell is initially equipped with an internal timer by randomly assigning it a clock value between 1 and a maximum clock value τ. We define a refractory period R such that $0 \leq R < \tau$ (see a detailed description of the internal timer, below). If the internal timer ϕ of a cell is less than R, the cell is in a refractory phase. Otherwise, the cell is sensitive. The local rules for myxobacterial cells are as follows:

(i) At each time-step, the internal timer of each refractory cell is increased by 1 while the internal timer of sensitive cells is increased by an amount proportional to the number of head-on cell–cell collisions n occurring at that timestep.
(ii) When a cell's internal timer has increased past τ, the cell reverses, the internal timer resets to 0 and the cell becomes refractory. Reversals occur as a cell's center switches from a right- or left-directed channel to a left- or right-directed channel, respectively.
(iii) During the final transport step, all cells move synchronously one node in the direction of their velocity by updating the positions of their centers. Separate velocity states at each node ensure that more than one cell never occupies a single channel.

Our model forms a stable ripple pattern from a homogeneous initial distribution for a wide range of parameters, with the ripples apparently differing only in ripple wavelength, ripple density and ripple width (see Fig. 3).

We find that C-signaling plays an important role in modulating cell density during rippling, and non-C-signaling cells have no effect on the rippling pattern when mixed with wild-type cells. Further, a refractory period is required for rippling

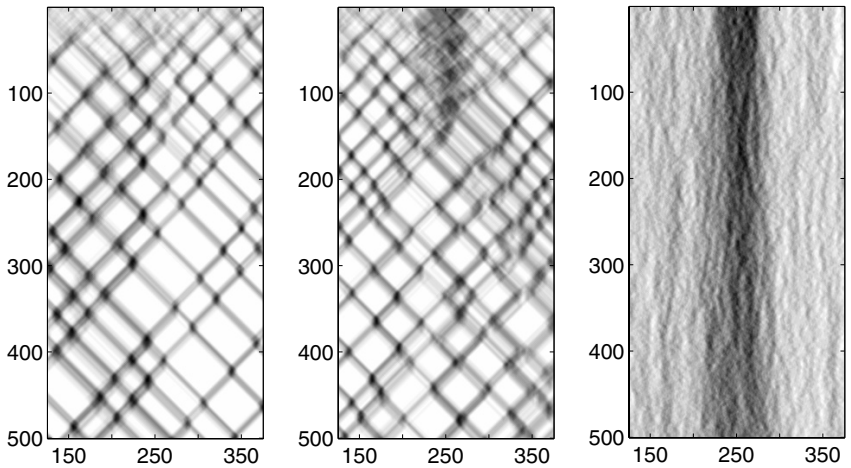

Fig. 4. Cell density over the third row of a 5×500 lattice over the first 500 time-steps for different initial conditions. Time increases as the vertical axis descends. (a) Cells are initially randomly distributed with density 3. Cell length = 5 nodes, $R = 10$ nodes, $t = 15$ nodes and $\tau = 2000$. (b) Same as in (a), but with a central stripe of density 15 and width 50 initially added vertically down the lattice. (c) Same as in (b), but cells are assigned random orientations at every time-step. (From Ref. 1 with permission.)

for cells of length greater than two or three nodes, and although there may exist a minimum response time of more than one time-step, it is an interesting result of our model that the minimum response period must be small compared to the refractory period. By comparing model results with experiments, we can conclude reversals during rippling would not be regulated by a built-in maximum oscillation period.

As density increases, wavelength decreases and the larger number of cells are distributed over a greater number of ripples. This result provides further evidence of the the role C-signaling plays as a density-sensing and density-modulating mechanism. To test this idea further, we ran a simulation for initial conditions in which a high density stripe stretches vertically down a lattice. As ripples formed and propagated, the cells were quickly distributed more evenly over the lattice (Fig. 4(b)). The redistribution of cells occurs much faster than if cells just perform random-walk (compare Figs. 4(b) and (c)). Thus, although there is no net transport of cells larger than one wavelength when cells are evenly distributed [29], there is a net migration of cells away from high density regions through the rippling process.

3.2. *Streaming*

Following the rippling stage, when cells have accumulated enough C-signaling molecules on their surfaces, instead of reversing in response to C-signal exchange, they suppress reversal and continue to move in the same direction. In fact,

they turn preferentially to directions that increase their level of C-signaling. We model myxobacteria aggregation starting from randomly distributed cells (without rippling).

Cells are modeled as 3×21 rods on a triangular lattice with periodic boundary conditions, as shown in Fig. 2(b) [3]. Cells first turn stochastically 60 degrees clockwise or counter-clockwise, or stay in their current direction. The local rule favors directions that maximize the overlap of the C-signal exchange neighborhood at the head of a cell with the C-signal exchange neighborhoods at the tails of neighboring cells. The probability for a given cell with orientation θ to turn in the direction of θ' is

$$P = \begin{cases} \dfrac{e^{\beta C(\theta')}}{Z(\theta)}, & \text{if } \theta' = \left(\theta, \theta + \dfrac{\pi}{6}, \theta - \dfrac{\pi}{6}\right), \\ 0, & \text{otherwise.} \end{cases}$$

where $C(\theta')$ is the amount of C-signaling if the cell is oriented at angle θ', the normalization factor $Z(\theta) = e^{\beta C(\theta)} + e^{\beta C(\theta+\frac{\pi}{6})} + e^{\beta C(\theta-\frac{\pi}{6})}$, with $\beta = 0.5$. This rule causes cells to align, which is a simplification of the hypothesis that alignment and C-signaling reinforce each other (see Refs. 14, 19 and 22). On the second step, all cells move synchronously one node in the directions of their corresponding velocities by updating the positions of their centers.

Cells aggregate in two distinctive stages in our simulations. During the first stage, cells turn from low density areas towards areas of slightly higher cell density. Initially randomly distributed cells condense into small stationary aggregates (Fig. 5(a)) which grow and absorb immediately surrounding cells. Next, some adjacent stationary aggregates merge and form long, thin streams which extend and shrink on their own or in response to interactions with other aggregates (Fig. 5(b)). These streams are transient and eventually disappear, leaving behind a new set of larger, denser stationary aggregates which are stable over time (Fig. 5(c)). Figure 5(d) shows an experimental figure in which two aggregates are interacting via a stream.

We measured the areas and densities of every stationary aggregate which appeared over the course of two simulations. These aggregates fall within a narrow region in the area-density phase diagram shown in Fig. 6(a), which we call an attractor region. As this attractor region covers a continuous rather than disconnected space, the different aggregate structures can continuously transform from one to the other. We perturb a stable aggregate in two ways. First, we study an adiabatic perturbation by gradually adding cells to an initially small, isolated aggregate. As cells are slowly added, the aggregate increases in area and density while remaining within the attractor region (Fig. 6(b)). The oscillation of the path in the wider region of the attractor corresponds to "pulsing" of an aggregate. Second, we introduce a non-adiabatic perturbation by placing two duplicate aggregates in close proximity of each other, which creates a new aggregate with double the initial area and the same density. Over 600 timesteps, this aggregate gradually reorganizes so

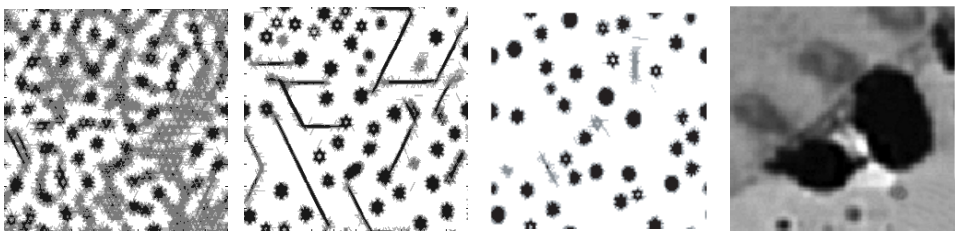

(a) (b) (c) (d)

Fig. 5. Aggregation stages on a 500×500 lattice, which corresponds to an area of 2.8 cm^2. Local cell density after (a) 200, (b) 900, and (c) 25,000 timesteps. Average cell density is 10. The number of simulated cells is 39,507. The darker shade of gray corresponds to higher cell density. (From Ref. 3 with permission). (d) The formation of a stream between two experimental *M. xanthus* aggregates on the edge of a submerged agar culture after 28 hours of starvation. (From Ref. 17 with permission.)

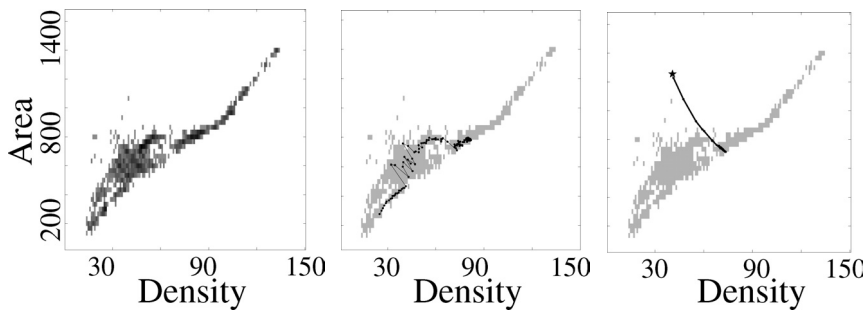

(a) (b) (c)

Fig. 6. Area-density phase diagram for (a) 186 stationary aggregates identified within two simulations over 25,000 timesteps, (b) an initially small aggregate to which cells are slowly added over 1,000 timesteps, and (c) an artificially constructed aggregate (star) over 600 timesteps. Relaxation of perturbation data in (b) and (c) are plotted every 10 timesteps on top of (a). (From Ref. 3 with permission.)

that it has an area and density within the stable region (Fig. 6(c)). Results from applying both kinds of perturbations suggest that the attractor region is stable.

To evaluate the role of internal noise, we devise a corresponding deterministic model. Instead of using a probabilistic rule to model cell turning, we use the following function to decide on the cell orientation for the next step:

$$f_i(r, k+1) = f_i(r - c_i^{\ominus}, k)\Omega(r - c_i^{\ominus}, k, c_i) + f_i(r - c_i^{\oplus}, k)\Omega(r - c_i^{\oplus}, k, c_i) + f_i(r - c_i, k)\Omega(r, k, c_i),$$

where f is the particle density distribution function over each lattice node r, k is the timestep, and c_i, $c_i^{\ominus}$, and $c_i^{\oplus}$ represent vectors in the ith direction, vectors turning clockwise from the ith direction, and vectors turning counter-clockwise respectively.

The collision function $\Omega(r, k, i)$ is the probability of a cell at the node r turning towards direction i at the kth timestep. We drop the exclusion principle so that the density of cells may be greater than 1 at a node. This function effectively converts our stochastic model based on cell turning into a deterministic model, analogous to the process of changing a stochastic lattice gas model to a deterministic lattice Boltzmann model.

Our simulations from Refs. 3 and 4 show that this deterministic model evolves similarly to the stochastic model, indicating that the aggregation dynamics are not sensitive to internal noise. Namely, many small aggregates appear, then streams form between interacting aggregates. Eventually the streams dissolve and leave behind a larger set of aggregates. One important difference is that streams in the deterministic model are fewer and smaller. Another difference is that streams are shorter-lived, and the deterministic simulation reaches a steady state much faster. These differences have a critical effect on the way aggregates reorganize. Comparing the size distribution of aggregates in the stochastic model with that of the deterministic model, we see that with the internal noise, aggregates can reach larger sizes. This is not surprising because noise slows the process of stream contraction so that streams persist longer and span a greater area, which enables more aggregates to interact and form larger, more stable aggregates.

3.3. *Aggregation*

We have also designed the first 3D model for myxobacteria aggregation [32] by extending local rules from a 2D model to a 3D case. There are 12 channels at each node of an 3D lattice. In our model cells can bend and have cell pole overlap with different overlapping sizes (see Fig. (2c)).

The cells are initially randomly distributed both in spatial directions and orientations. Even though all cells in our model follow the same simple set of rules, several different patterns emerge. At first, cells form patches, within which cells have predominantly the same orientation. Near the intersection of two patches, cells stall as they are prevented from turning by other cells (Fig. 3(a)), resulting in a 2D structure called a traffic jam. The jam formation is purely mechanical. Cells which are not in the immediate vicinity of such jams can form streams, in which cells align with each other and move in the same direction. In time, due to cell streaming, not all of the 2D jammed structures survive. Some of them dissipate by joining streams moving toward other jammed structures, resulting in bigger 3D asymmetric stationary aggregates (Fig. 7(d)). As a stream of cells approaches a traffic jam, they glide around or over the jam, as if it were an inanimate lump. The cells must bend as it passes over or around the jam, and thus initiates a roughly circular orbit, or a "skirt" (Fig. 7(c)).

Elongated cells with a wide range of aspect ratios aggregate around a frozen traffic jam and created a "skirt" followed by a 3D mound. Shorter and rounder cells cannot aggregate.

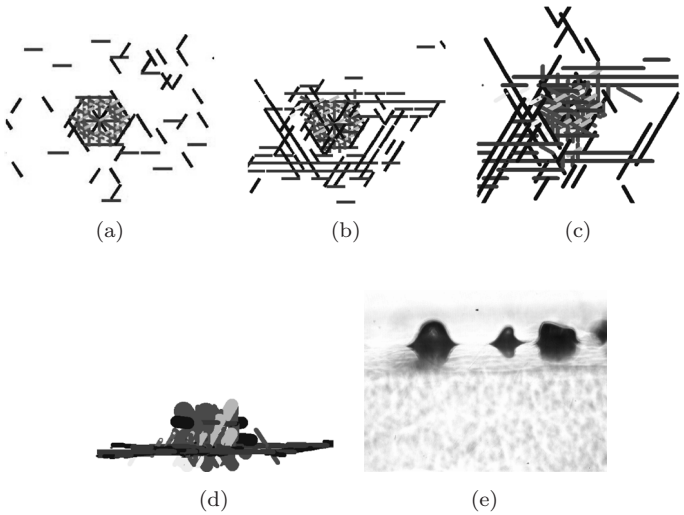

Fig. 7. Snapshots of aggregation phases. In (a) cells form a traffic jam. Some cells circulate around jam in both directions, forming motile "skirt" (b), and some of them glide over jam and get "stuck" (c). This results in a bell-shaped aggregate (d) (side view). (e) Experimental photo of *M. xanthus* fruiting bodies in a side view. (From Ref. 32 with permission.)

3.4. *Sporulation and fruiting body formation*

Vegetative myxobacteria cells in large stable aggregates differentiate into round environmentally-resistant spores, and eventually build complex multicellular fruiting bodies. Internally a nascent fruiting body consists of two concentric domains. An outer motile shell with high cell density surrounds a three times less dense hemispherical mound [27, 28]. Differentiation of elongated motile cells into spherical spores begins in outer domain which is densely packed with circling cells. During sporulation cells lose their gliding motility [27]. Therefore, spores need some external force applied to them in order to move toward inner domain as seen in the experiment. Motile rod-shaped cells, still remaining in outer shell, can provide such external transport for spores by mechanically pushing spores during their circular motion [27].

In our 3D model, cell differentiation in a mature aggregate starts when C-signaling of individual cells reach a certain threshold value. As was mentioned before, an elongated cell is represented as a rotational ellipsoid with short half-axes of 1.5 units and a long half-axis of 5.5 units (Fig. 2(c)). To preserve the cell volume we represent a spore as a sphere with the radius of about 2.3 units. Simulations demonstrate that spores first appear in the "skirt" (outer region) of an aggregate. The number of spores increases with time and spores are pushed mechanically by moving cells as a result of elastic collisions.

As cells glide they also secret a sticky slime behind them and lubricate the rough surface. Cells prefer to glide along the slime tracks. In our model every cell deposits slime on the bottom level of the lattice and probability of a cell turning in

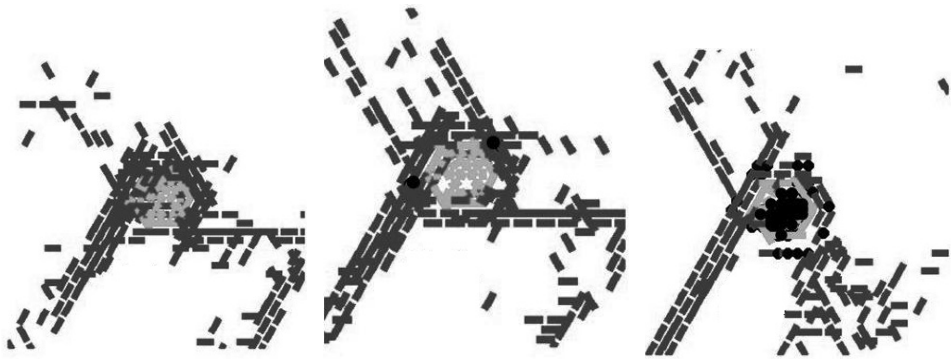

(a) (b) (c)

Fig. 8. Spore formation and transport. (a) Multicellular myxobacteria aggregate: inner domain (lighter shade) and outer domain (darker shade). (b) Initial spore precursors are formed in the outer domain (black spheres). (c) Spores are pushed by the elongated cells toward the inner domain where they accumulate.

the direction of an existing slime track is increased. The slime hardens after being exposed to air. Therefore, we use a "slime clock" so that after a prescribed time the slime track disappears. These rules together with high cell density and continuous cell movement result with time in an aggregate being completely covered with slime.

Spores are pushed in all possible directions but their motion is stabilized by slime. Simulations show that, in the presence of slime, most spores end up in aggregates' inner area (Fig. 8).

4. Discussion

In this paper, we reviewed a variety of biological lattice gas cellular automata models for different stages of myxobacteria fruiting body formation. In particular, we discussed hypothesis concerning mechanisms of cell morphogenesis, and demonstrated how cell-contact mediated signaling could allow myxobacterial communities to form complex morphologies.

We find that C-signaling and a refractory period are essential for rippling pattern formation. Rippling is an efficient mechanism for both forming evenly spaced accumulations of high cell density, and evenly spaced accumulations of nearly equal cell density.

The aggregates in our 2D simulations resemble the unique structures of several myxobacteria fruiting bodies. In *Myxococcus xanthus*, the basal region of the fruiting body is a shell of densely packed cells which orbit both clock-wise and counter-clockwise around an inner region only one-third as dense [15, 28]. In our model, typical simulation aggregates have this geometry and cell tracking demonstrates that cells orbit clockwise and anti-clockwise. Further, aggregates in our simulation often form in clusters of two or three closed orbits while in *Stigmatella erecta*, several fruiting bodies may form in groups and fuse [4, 26].

In experiments, one myxobacteria aggregate has been observed to mysteriously grow as an adjacent aggregate disappears. Our simulations offer a mechanism for this process: a stream may form connecting two adjacent aggregates and cells migrate from the smaller aggregate to the larger aggregate. Experimentally, these streams may not be visible if the density threshold for viewing cells is greater than the density found within the stream. Figure 5(d) shows a movie snapshot in which a barely visible stream has developed between two aggregates. Shortly after the formation of this stream, the two aggregates fuse. Streams effectively serve as a means for long-range communication between cells.

Our 3D model reproduces several stages of aggregation that have been experimentally observed, including non-symmetric, initial aggregates (traffic jams), streams, and hemispherical 3D mounds surrounded by a motile "skirt." The model demonstrates that the traffic jams can serve as initial "seeds" for aggregation, which then develop into mature 3D mounds. Our 3D simulations capture both the formation of a skirt around a traffic jam and the subsequent dissolution of the jam by cell bending and cell reversal. Then, cells from the jam joined the motile skirt. We also demonstrate the importance of cell polarity, showing that rod-like cells could aggregate, but spheres could not.

Further development of the aggregate into a mature 3D fruiting body require cell differentiation, in which rod-shaped myxobacteria differentiate into rounded spores that have lost the ability to move. By adding a sporulation mechanism based on the level of accumulated C-signal and passive spore transport provided by motile cells, we are able to simulate spores accumulation within an aggregate's inner area, thus capturing the beginning stage of the nascent fruiting body growth [33]. This approach will eventually enable us to develop a unified model for simulating all stages of the myxobacteria fruiting body formation.

Acknowledgments

Y. Jiang is partially supported by the National Nuclear Security Administration of the U.S. Department of Energy at Los Alamos National Laboratory under Contract No. DE-AC52-06NA25396. M. Alber and O. Sozinova are partially supported by the NSF grant 0622940 and NIH grant 1R0-GM076692-01.

References

[1] Alber, M. S., Jiang, Y. and Kiskowski, M. A., Lattice gas cellular automata model for rippling and aggregation in myxobacteria, *Physica D* **191**, 343–358 (2004).

[2] Alber, M. S., Kiskowski, M. A., Jiang, Y. and Newman, S. A., Biological lattice gas models, in G. Dangelmayr and I. Oprea (Eds.), *Dynamics and Bifurcation of Patterns in Dissipative Systems*, World Scientific Series on Nonlinear Science, Vol. 12 (World Scientific, Singapore, 2004), pp. 274–291.

[3] Alber, M. S., Kiskowski, M. A. and Jiang, Y., Two-stage aggregate formation via streams in myxobacteria, *Phys. Rev. Lett.* **93**, 068102 (2004).

[4] Alber, M. S., Jiang, Y. and Kiskowski, M. A., Role of streams in aggregation formation in myxobacteria, *Phys. Biol.* **1**, 173–183 (2004).
[5] Behmlander, M. B. and Dworkin, M., Extracellular fibrils and contact-mediated cell interactions in *Myxococcus xanthus, J. Bacteriol.* **173**, 7810–7821 (1991).
[6] Börner, U., Deutsch, A., Reichenbach, H. and Bär, M., Rippling patterns in aggregates of myxobacteria arise from cell–cell collisions, *Phys. Rev. Lett.* **89**, 078101 (2002).
[7] Burchard, R. P., Gliding motility of prokaryotes: Ultrastructure, physiology, and genetics, *Ann. Rev. Microbiol.* **35**, 497–529 (1981).
[8] Fiegna, F. and Velicer, G. J., Competitive fates of bacterial social parasites: Persistence and self-induced extinction of *Myxococcus xanthus* cheaters, *Proc. Roy. Soc. Biol. Sci. B.* **270**, 1527–1534 (2003).
[9] Keller, E. and Segel, L., Initiation of slime mold aggregation viewed as an instability, *J. Theor. Biol.* **26**, 399–415 (1970).
[10] Gronewold, T. M. and Kaiser, D. The act operon controls the level and time of C-signal production for *Myxococcus xanthus* development, *Mol. Microbiol.* **40**, 744–756 (2001).
[11] Igoshin, O. A., Mogilner, A., Welch, R. D., Kaiser, D. and Oster, G., Pattern formation and traveling waves in myxobacteria: Theory and modeling, *Proc. Natl. Acad. Sci. USA* **98**, 14913–14918 (2001).
[12] Igoshin O. A., Kaiser, D. and Oster, G., Breaking symmetry in myxobacteria, *Curr Biol.* **14**, 459–462 (2004).
[13] Jelsbak, L. and Søgaard-Andersen, L., Pattern formation: Fruiting body morphogenesis in *Myxococcus xanthus*, *Curr. Opin. Microbiol.* **3**, 637–642 (2000).
[14] Jelsbak, L. and Søgaard-Andersen, L., Pattern formation by a cell surface-associated morphogen in *Myxococcus xanthus, Proc. Natl. Acad. Sci. USA* **99**, 2032–2037 (2002).
[15] Julien, B., Kaiser, A. D. and Garza, A., Spatial control of cell differentiation in *Myxococcus xanthus*, *Proc. Natl. Acad. Sci. USA* **97**, 9098–9103 (2000).
[16] Kaiser, D., Building a multicellular organism, *Ann. Rev. Genet.* **35**, 103–123 (2001).
[17] Kaiser, D. and Welch, R., Dynamics of fruiting body morphogenesis, *J. Bacteriol.* **186**, 919–927 (2004).
[18] Kim, S. K. and Kaiser, D., Cell alignment required in differentiation of *Myxococcus xanthus*, *Science* **249**, 926–928 (1990).
[19] Kim, S. K. and Kaiser, D., C-factor has distinct aggregation and sporulation thresholds during *Myxococcus* development, *J. Bacteriol.* **173**, 1722–1728 (1991).
[20] Kruse, T., Lobedanz, S., Berthelsen, N. M. and Sogaard-Andersen, L., C-signal: A cell surface-associated morphogen that induces and co-ordinates multicellular fruiting body morphogenesis and sporulation in *Myxococcus xanthus*, *Mol. Microbiol.* **40**, 156–168 (2001).
[21] Kuner, J. M. and Kaiser, D., Fruiting body morphogenesis in submerged cultures of *Myxococcus xanthus*, *J. Bacteriol.* **151**, 458–461 (1982).
[22] Li, S., Lee, B. U. and Shimkets, L. J., CsgA expression entrains *Myxococcus xanthus* development, *Genes Dev.* **6**, 401–410 (1992).
[23] Lobedanz, S. and Søgaard-Andersen, L., Identification of the C-signal, a contact-dependent morphogen coordinating multiple developmental responses in *Myxococcus xanthus*, *Genes Dev.* **17**, 2151–2161 (2003).
[24] Lutscher, F. and Stevens, A., Emerging patterns in a hyperbolic model for locally interacting cell systems, *J. Nonlinear Sci.* **12**, 619–640 (2002).
[25] Nudleman, E. and Kaiser, D., Pulling together with type IV pili, *J. Mol. Microbiol. Biotechnol.* **7**, 52–62 (2004).

[26] Reichenbach, H., Biology of the myxobacteria: Ecology and Taxonomy, in *Myxobacteria II*, eds., Dworkin, M. and Kaiser, D. (American Society for Microbiology, Washington DC, 1993), pp. 13–62.

[27] Sager, B. and Kaiser, D., Spatial restriction of cellular differentiation, *Genes. Dev.* **7**, 1645–1653 (1993).

[28] Sager, B. and Kaiser, D., Two cell-density domains within the *Myxococcus xanthus* fruiting body, *Proc. Natl. Acad. Sci.* **90**, 3690–3694 (1993).

[29] Sager, B. and Kaiser, D., Intercellular C-signaling and the traveling waves of *Myxococcus*, *Genes. Dev.* **8**, 2793–2804(1994).

[30] Shimkets, L. J. and Kaiser, D., Induction of coordinated movement of *Myxococcus xanthus* cells, *J. Bacteriol.* **152**, 451–461 (1982).

[31] Sproer, C., Reichenbach, H. and Stackebrandt, E., The correlation between morphological and phylogenetic classification of myxobacteria, *Int. J. Syst. Bacteriol.* **49**, 1255–1262 (1999).

[32] Sozinova, O., Jiang, Y., Kaiser, D. and Alber, M., A three-dimensional model of myxobacterial aggregation by contact-mediated interactions, *Proc. Natl. Acad. Sci.* **102**, 11308–11312 (2005).

[33] Sozinova, O., Jiang, Y., Kaiser, D. and Alber, M., A three-dimensional model of myxobacterial fruiting body formation, *Proc. Natl. Acad. Sci. USA* **103**, 17255–17259 (2006).

[34] Welch, R. and Kaiser, D., Cell behavior in traveling wave patterns of myxobacteria, *Proc. Natl. Acad. Sci. USA* **98**, 14907–14912 (2001).

[35] Wolgemuth, C., Hoiczyk, E., Kaiser, D. and Oster, G., How myxobacteria glide, *Curr. Biol.* **12**, 369–377 (2002).